Ostwald ripening of two-dimensional islands on Si(001)

N. C. Bartelt*
Department of Physics, University of Maryland, College Park, Maryland 20742

W. Theis† and R. M. Tromp
IBM Research Division, Thomas J. Watson Research Center, P.O. Box 218, Yorktown Heights, New York 10598
(Received 11 December 1995)

We have used low-energy electron microscopy to study two-dimensional island ripening on Si(001). By studying the behavior of individual islands compared to their surroundings, we are able to quantify the step-edge attachment and terrace diffusion processes that are responsible for the ripening. By comparing the time dependence of specific configurations of islands to simulations, we find correlations in the rate of change of an island's area with the sizes of neighboring islands, implying that the chemical potential of the adatom sea is not uniform as classical theories of Ostwald ripening assume. From measurements of the time dependence of each island, we chart out these nonuniformities and relate them to adatom diffusion coefficients. [S0163-1829(96)01940-6]

I. INTRODUCTION

During epitaxial growth, islands of the growing material nucleate if the distance between steps is sufficiently large. The surface is out of equilibrium since the step edges of the islands cost free energy. When growth is terminated, atoms flow from steps with high curvature to steps with low curvature: small islands shrink until they disappear, while large islands grow at their expense. This coarsening process, called Ostwald ripening,[1] is a general feature of the late stages of phase separation. Understanding the ripening of islands is clearly a necessary first step in understanding the much more complex issues involved in epitaxial growth.

In this paper we explore the ripening of two-dimensional (2D) islands on Si(001).[2] Our goal is to account quantitatively for *in situ* observations of the evolution of the island configuration on an island-by-island basis. Understanding how each island behaves in response to its surroundings depends upon several factors. Atoms, probably in the form of dimers on Si(001), detach from small islands, diffuse through the adatom sea surrounding the islands, and eventually attach to larger islands. The net rate of attachment or detachment from each island depends on the chemical potentials of the surrounding adatom sea, as well as the chemical potentials of the atoms in the islands and the barrier to attachment and detachment.

There are two extreme possibilities for the behavior of the chemical potential of the adatom sea near an island edge. If the random exchange between the adatom sea and the island edge is sufficiently rapid, then the adatom sea immediately surrounding each island will always be in thermal equilibrium with the atoms in the island. The net flow of atoms towards or away from each island will then be completely determined by diffusion in the chemical potential gradients of the surrounding adatom sea. On the other hand, if detachment and attachment are slow compared to diffusion, then the adatom chemical potential can be out of equilibrium with the island edge and net detachment rates will be determined by the difference between the chemical potential of the adatom sea and the chemical potential of atoms in the island.

Previous low-energy electron microscopy (LEEM) studies of step fluctuations on Si(001) (Ref. 3) have shown that thermal step fluctuations on Si(001) are limited by attachment and detachment kinetics. In this work we will show that the evolution of island configurations during ripening, as well as the dissolution of isolated islands, is also limited by attachment and detachment kinetics, allowing for a consistent description of these phenomena. Furthermore, expanding on Ref. 4, we will show that the previous quantitative measurements of step-edge stiffnesses and the step edge mobility, which determine how fast steps move when out of equilibrium with the adatom sea, yield predictions of island ripening and dissolution rates that are consistent with the LEEM observations of island ripening presented here.

In general, one expects that how each island behaves will depend on the detailed configuration of the surrounding islands. Classical mean-field theories,[5] which make the assumption that the adatom chemical potential surrounding each island is the same and determined by the average island size, are exact only when diffusion becomes infinitely fast[6] or in the limit of an infinitesimally small fraction of the surface covered by islands.[1] The local correlations between islands that can cause the chemical potential of the adatom sea to become nonuniform and thus cause an island's behavior to depend on the details of its environment are the subject of quite a few theoretical studies.[1,7–10] However, most experimental evidence[8,11] for local correlations in Ostwald ripening comes indirectly, through broadening of the island-size distribution compared to the mean-field distributions, or though interpretation of static island-size correlation functions.[12] Here, by using LEEM to image the evolution of individual islands, we can map out the chemical potential of the adatom sea and thereby explicitly show the presence of correlations and quantitatively relate them to an adatom diffusion constant.

The plan of this paper is as follows. First, the LEEM experiment and how the data were analyzed are described in Sec. II. Next, in Sec. III, the time dependence of the average

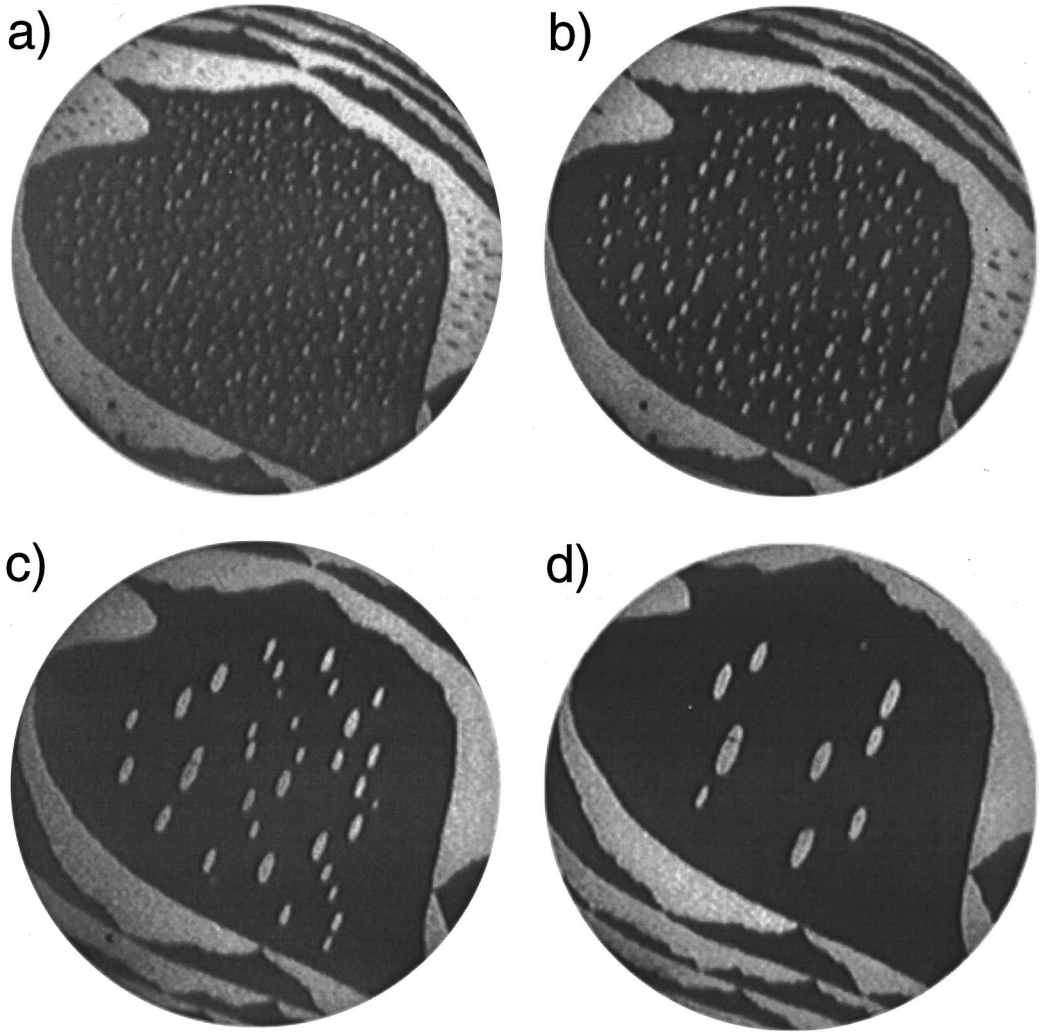

FIG. 1. LEEM images of ripening of single atomic layer height islands on Si(001) at various times after the temperature was increased to 670 °C: (a) 10 s, (b) 50 s, (c) 400 s, and (d) 1300 s. Alternate dark and bright regions differ in height by one atomic layer (0.096 nm). The field of view is 5.5 μm.

island size and the distribution of sizes is discussed. This average behavior is shown to be consistent with step-edge kinetics limited by step edge attachments. The behavior of isolated islands as they dissolve, presented in Secs. IV and V, confirms this picture. In Sec. VI the observed step edge kinetics is discussed in the light of previous LEEM and scanning tunneling microscopy (STM) work. Detailed simulations of the time evolution of specific island configurations are presented in Sec. VII. These establish that the ripening of each island is determined by the sizes of neighboring islands rather than by the average sizes of all the islands, as in standard mean-field theories. In Sec. VIII, LEEM data are used to map out the spatial dependence of the adatom chemical potential, and the nearest neighbor model is shown to account for the variation. Section IX provides an explanation for the success of the nearest-neighbor model by taking diffusion into account explicitly.

II. EXPERIMENT

The ripening experiment was performed on a Si(001) surface with a 5-μm-sized step-free region. Approximately 0.1 monolayer of Si was deposited at room temperature, creating a disordered overlayer. The temperature was then rapidly increased to, and stabilized at, 670 °C. The subsequent evolution of the surface morphology was observed by LEEM (Ref. 13) and recorded on video tape. Figure 1 shows the ripening of the resulting island configuration at four different times after the temperature reached 670 °C. The image contrast is due to the (2×1) dimer reconstruction on the Si(001) surface. The dimer reconstruction rotates by 90° when the surface height changes by one atomic layer. In the dark field imaging mode used in Fig. 1, terraces with one dimer orientation appear dark, while the perpendicular orientation appears bright. Thus the bright elliptical islands are one atomic layer higher than the surrounding dark terrace. In separate experiments at higher temperatures, the behavior of isolated islands formed during the late stages of the ripening on similarly sized terraces was studied. The results of these experiments are summarized in Sec. IV.

To analyze the video sequences, we digitized the video at a rate of one frame per second. Islands were marked by converting each video frame into a binary black-and-white image by thresholding the images at an appropriate intensity level.[14] The area and center of mass of each island was then

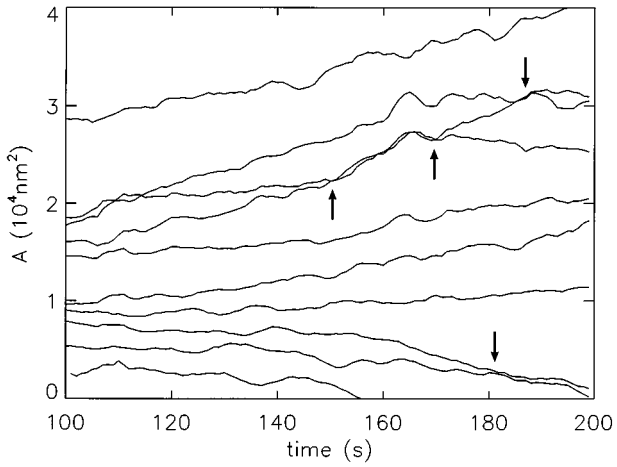

FIG. 2. Time dependence of the areas of a few of the islands. Large islands grow; small islands shrink. During the time period covered by this figure, there are around 100 islands and the total island area decreases by only about 5%. The arrows indicate points where islands of initially different sizes have evolved to islands of the same area or where the areas of islands of the same size have begun to diverge.

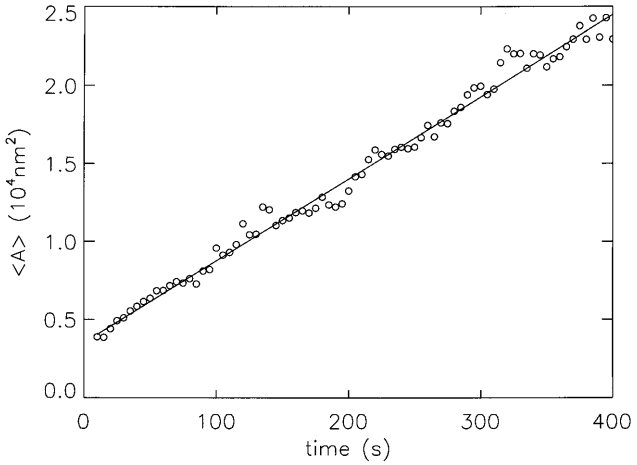

FIG. 3. Time dependence of the average island area during ripening at 670 °C. The linear increase is consistent with detachment limited kinetics.

computed. After the surface was at 670 °C for 10 s [Fig. 1(a)], there were approximately 300 well-defined islands; 22 min later [Fig. 1(d)] there were 11. Except for rare cases when the islands contain (2×1) domain boundaries because of island coalescence, the islands are all ellipses with an aspect ratio of ≈ 2.6.[3] The (2×1) dimer rows run along the long dimension of the ellipses. Except for islands near the bounding step edge, there is no measurable shift of the centers of mass of the islands with time. The percentage area of the large terrace covered with islands drops from 7.4% after 50 at 670 °C to 5.7% after 400 s. In the few islands where (2×1) domain boundaries occurred, the boundaries were expelled by a slow consistent motion towards the ends of the ellipses. After 50 s at 670 °C, island coalescense was absent.

Figure 2 shows the time dependence of the area of a few of the islands, showing explicitly the ripening process. Small islands tend to shrink and large islands tend to grow, with the largest islands growing the fastest. Because the total island area on the terrace during the time period of the figure only changes by 0.4% of a monolayer, the shrinkage of the small islands is closely balanced by the growth of the large islands. As a first approximation, how fast an island grows or shrinks depends only on its size. However, a few clear examples of the failure of this approximation are pointed out in the figure: islands with initially different areas evolve to islands of the same size, indicating that islands with the same size have different rates of change.[15] As we will discuss later, these differences can be attributed to particular variations in the configurations of neighboring islands.

III. THE DISTRIBUTION OF ISLAND SIZES

We first discuss the time evolution of quantities averaged over the island configuration. Figure 3 shows the observed time dependence of the average island area. To a good approximation, it increases linearly with time. As first recognized for 3D Ostwald ripening by Wagner,[16] this linearity is consistent with step-edge motion that is limited by attachment and detachment reaction kinetics at the step edge. It is clearly inconsistent with the $t^{2/3}$ time dependence that characterizes step motion which is solely limited by diffusion away from the step edge.[5,7]

That the ripening is reaction limited also has effects on the static island size distribution. Figure 4 shows the distribution of island sizes at three times, compared with the long-time distributions predicted by mean-field theories of the ripening. As expected from scaling theories,[5,16] the experimental distribution does not change significantly with time, although statistics become poorer at later times. The observed distributions are clearly much broader than predicted by the 2D Lifshitz-Slyosov theory of purely diffusion-limited ripening. They are, however, very similar to the detachment-attachment limiting case. (For convenience, the mean-field expressions for this case are given in the Appendix.) Interpreting these distributions is complicated by the fact that the mean-field theory of diffusion-limited ripening is only exact in the limit of the total island coverage becoming small. Higher coverages cause a broadening of the size distribution, and thus distributions broader than the Lifshitz-Slyosov theory are often interpreted as a signature of the failure of mean-field theory.[8] In the light of Fig. 3, here we take the broad distribution as a manifestation of attachment-limited kinetics.

IV. DECAY OF ISOLATED ISLANDS

To interpret the ripening more quantitatively, we begin by defining the step mobility and relating it to the decay of isolated islands. If, as is the case for Si(001), the behavior of an island depends on the rate of attachment and detachment at the step edge, then the total flux from each island edge will be proportional to the difference between μ, the chemical potential of the atoms composing the island, and μ_{ad} the chemical potential of the adatom sea surrounding that island. Defining the step mobility Γ by the proportionality

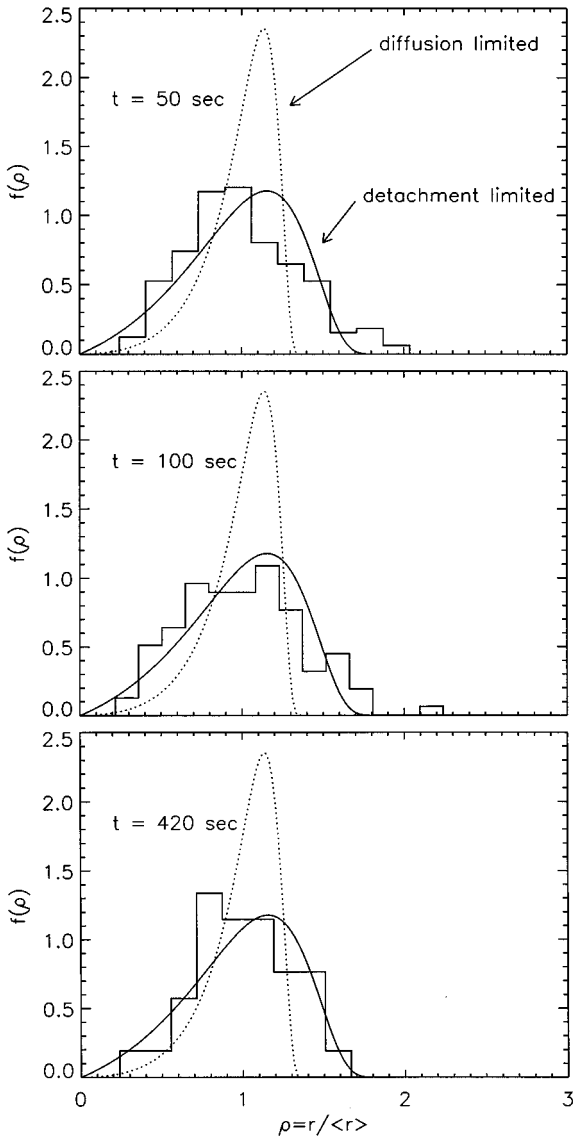

FIG. 4. Normalized experimental distributions of island sizes at 50 s, 100 s, and 420 s, compared with the predictions of mean-field theories of Ostwald ripening. The dotted lines correspond to low-coverage ripening limited by diffusion in the adatom sea surrounding the islands. The solid line, which shows much better agreement with the data, is the distribution for attachment limited kinetics [Eq. (A3)].

constant,[17,18] the rate of change of island area A is given by

$$\frac{\partial A}{\partial t} = -\frac{C\Gamma}{\omega kT}(\mu - \mu_{\mathrm{ad}}), \tag{4.1}$$

where C is the island circumference and ω is the area of an adatom. For elliptical islands with semimajor and minor axes of length R_A and R_B, $C \approx 2\pi\sqrt{(R_A^2+R_B^2)/2}$. The Gibbs-Thomson chemical potential of an elliptical island is

$$\mu = \omega\sqrt{\frac{\tilde{\beta}_A\tilde{\beta}_B}{R_A R_B}} = \omega\sqrt{\frac{\pi\tilde{\beta}_A\tilde{\beta}_B}{A}}, \tag{4.2}$$

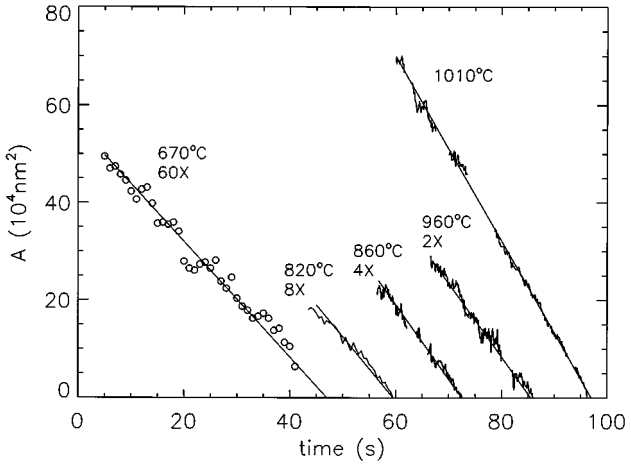

FIG. 5. Time dependence of the area of large isolated islands at various temperatures from 820 °C to 1010 °C. The points for 670 °C correspond to the average over ten islands as they are about to disappear during the ripening sequence of Fig. 1. As discussed in the text, the linear decrease in area with time is characteristic of step-edge motion limited by step-edge detachment kinetics.

where $\tilde{\beta}_A$ and $\tilde{\beta}_B$ are the step-edge stiffnesses for steps running perpendicular to the major and minor axes of the elliptical island shapes. When the island size is sufficiently small, the adatom chemical potential can be neglected and the island area decreases linearly in time:

$$\frac{\partial A}{\partial t} = -\frac{2\pi\Gamma}{kT}\sqrt{\frac{\tilde{\beta}_A\tilde{\beta}_B}{2}\left(\frac{R_A}{R_B}+\frac{R_B}{R_A}\right)}. \tag{4.3}$$

We have checked this relationship over a wide range of temperatures. Figure 5 shows the time dependence of large isolated islands on a 4-μm terrace from 820 °C to 1010 °C. Also plotted for 670 °C is the decay of the average area of ten small islands. The linear behavior observed at all temperatures is consistent with the attachment limited kinetics of Eq. (4.3) and clearly inconsistent with the $t^{2/3}$ dependence predicted for purely diffusion-limited island dissolution. As discussed in Secs. V and VI, the slope of these lines is consistent with the value of the step mobility needed to explain the overall ripening rates, as well as the time scale of previously observed capillary wave motion.

V. RELATIONSHIP BETWEEN ISOLATED ISLAND DISSOLUTION AND OVERALL RIPENING RATES: COMPARISON WITH MEAN-FIELD THEORY

The (experimentally) determined rate of area decrease of small islands fully determines via Eqs. (4.1) and (4.3) how any island will ripen, depending upon its size and the local chemical potential of the adatom sea. To understand the time dependence of the ripening, we thus need to know what determines μ_{ad}. One might suppose, for example, that because of fast diffusion, the entire adatom sea is close to equilibrium with the almost straight bounding step (i.e., $\mu_{\mathrm{ad}} \approx 0$) and smaller than the chemical potentials of all the islands on the terraces. Then, however, all of the islands would dissolve at a similar rate [Eq. (4.3)]. This situation is in obvious dis-

agreement with the experiment in which a significant number of islands actually grow in size. The value of μ_{ad} must be higher and determined by the distribution of islands on the terrace. In the Appendix it is shown that if one makes the mean-field assumption that μ_{ad} is uniform, then in the limit of a large number of islands μ_{ad} is the chemical potential of an island with the average radius and the rate of increase in the average area is 1/3.6 of the single island dissolution rate. (The effect of the bounding step edge becomes small as the number of islands gets large.) Fitting the disappearance of ten islands to a line yields a dissolution rate of $1.9\pm0.4\times10^2$ nm^2/s. From Fig. 3, the average island growth rate is 0.50×10^2 nm^2/s. The ratio is 3.8 ± 0.8, in fair agreement with mean-field theory. In Sec. VII below we will show, in spite of this agreement, that this mean-field theory, which ignores the possibility of variations in the chemical potential due to the correlations between the evolution of neighboring islands and the effect of the proximity of the bounding step edge, fails to explain the time dependence of individual islands in the configuration.

VI. STEP-EDGE MOBILITY

A more complete picture of the kinetic processes governing the island dissolution can be obtained by using the dissolution rate in combination with our previous analysis of thermal step fluctuations on Si(001).[3] The islands are continually exchanging adatoms with the adatom sea. This (random) exchange causes step positions to fluctuate. These fluctuations have been analyzed to obtain adatom exchange rates.[3] As we will show quantitatively below, the random exchange rates deduced from this analysis are much greater than the total island dissolution rates. This finding is significant because large exchange rates allow the step structure to be in local equilibrium as the island edges move, which is a necessary condition for the validity of approaches based on Eq. (4.1). Also, and perhaps more importantly, since the magnitude of the bias in the exchange rate when the step is slightly out of equilibrium is determined by the mobility, which is deduced from the equilibrium rates, characterizing the large random exchange rate is essential for understanding how the steps move when they are out of equilibrium. Indeed, we will show that the previously measured random exchange rates are consistent with the observed island dissolution rates.

From theories of thermal step fluctuations,[19] the step mobility Γ which appears in Eq. (4.1), is approximately $\omega^{3/2}/\tau$, where τ is the time between random attachments or detachments at an arbitrary position on the step edge. Analysis of the Langevin equation appropriate for attachment-limited step fluctuations[20] reveals that the decay time $\tau(q)$ for a fluctuation with wave number q is $kT/\Gamma\tilde{\beta}q^2$. On the other hand, the amplitude of thermal fluctuations due to equipartition of energy among the step capillary modes is independent of Γ and equal to $kT/\tilde{\beta}q^2$. Thus the ratio of the amplitude to $\tau(q)$ should be equal to Γ, independent of q. Figure 6 shows Γ estimated from this ratio at 860 °C for various q using the data and analysis of Si(001) step fluctuations described in Ref. 3. These estimates of Γ are indeed approximately independent of q and thus consistent with the simple step attachment limited kinetics deduced from Fig. 6.

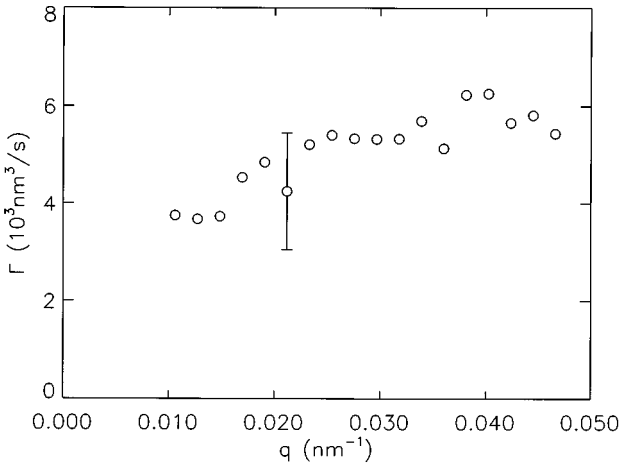

FIG. 6. Plot of the step mobility Γ as function of wave number q for S_B step capillary waves at 860 °C, as determined by the data and analysis presented in Ref. 3. The size of the error bar reflects the statistical variation observed for different analyzed steps.

(If, on the other hand, the step fluctuations were limited by diffusion in the adatom sea, then Γ estimated in this way should vanish linearly in q at small q,[21] which is definitely not consistent with the data.)

The particular value of the mobility, 4×10^3 nm^3/s, deduced from Fig. 6 is interesting for two reasons. First, it corresponds to around 23 000 random dimer attachments and detachments per second,[22] per dimer along the step edge. For comparison, the observed dissolution rate for an island of area 2×10^4 nm^2 at 860 °C of 3.8×10^3 nm^2/s corresponds to 32 dimer detachments per second per boundary dimer. As stated above, the validity of Eq. (4.1) requires that the net motion of the step edge is much smaller than the random motion.[23] At the ripening temperature of 670 °C, both rates are approximately 10 times slower. Because the random Brownian motion of steps determines how fast a step configuration diffuses towards equilibrium though Eq. (4.1), the step fluctuations can be used to predict the dissolution rate. Using the step stiffnesses of $\tilde{\beta}_A=0.9$ kT/nm and $\tilde{\beta}_B=0.13$ kT/nm deduced in Ref. 3 and the above value of Γ in Eq. (4.3), we predict a dissolution rate of 10×10^3 nm^2/s compared with the observed 3.8×10^3 nm^2/s. This factor-of-2 agreement (which is within the errors of determining Γ) is encouraging evidence that the picture presented here of the step mobility is correct.[24]

Figure 7 compares the temperature dependence of the step mobilities extracted from the step fluctuations[3] with the mobilities obtained from measuring the island dissolution rates. Although there is a consistent factor-of-2 difference, the activation energy for both mobilities are within uncertainties the same: 1.45 ± 0.15 eV. Extrapolating the Arrhenius plots down to 475 °C yields a dimer exchange rate with the step edge of order one per second, consistent with STM observations.[25–28] The activation energy is consistent with the 1.4–1.7 eV range extracted from STM step-edge attachment rates observed at lower temperature by Kitamura *et al.*,[27] consistent with the 1.3 ± 0.3 eV quoted by Swartzentruber and Schact,[28] although significantly larger than the value 0.97 ± 0.12 reported by Pearson *et al.*[26]

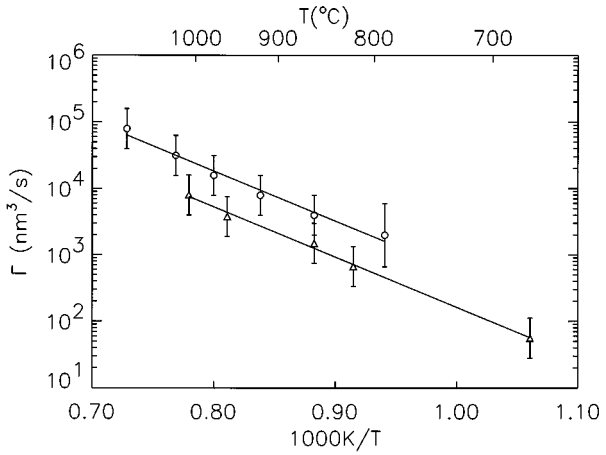

FIG. 7. Arrhenius plot of the step mobility Γ obtained from step fluctuation (circles), compared to the mobilities obtained from the island dissolution rates (triangles). The deduced activation energy for both methods is 1.45 ± 0.15 eV.

VII. SIMULATIONS OF ISLAND CONFIGURATIONS

We now show that while mean-field theory can explain very well the average behavior shown in Figs. 3 and 4, it fails in predicting the detailed time dependence of the actual configuration of islands. Some suggestion that mean-field theory fails has already been shown by the existence of intersecting lines pointed out in Fig. 2, which show that growth and dissolution rates do not depend only on island size as mean-field theory predicts. To show how serious these failures are in determining the island configurations, we have performed simulations where we take an experimental configuration, propagate it forward in time, and compare the results to what actually happens.

Figure 8 shows the experimental configurations at three different times, which will be compared with theory. Figure 9 shows what happens when the experimental island areas at 50 s are propagated forward in time according to Eqs. (4.1) and (4.2),[29] with the mean-field assumption of a uniform $\mu_{\rm ad}$ equal to the Gibbs-Thomson chemical potential of the average island radius at each time step in the simulation, ignoring the bounding step edge. The value of Γ used, 56 $\rm nm^3/s$, is that inferred from the single island dissolution rate. Comparing with Fig. 8 shows serious problems with mean-field theory: the islands near the center of terrace disappear much more quickly than experiment.

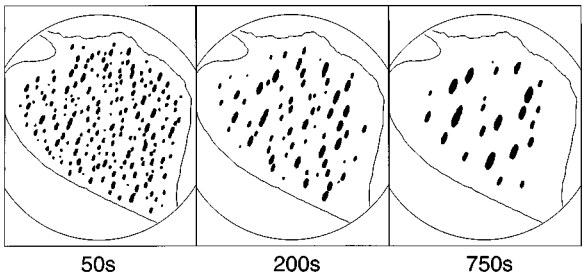

FIG. 8. Marked island configurations at three times. These configurations are compared with theory in Figs. 9 and 10.

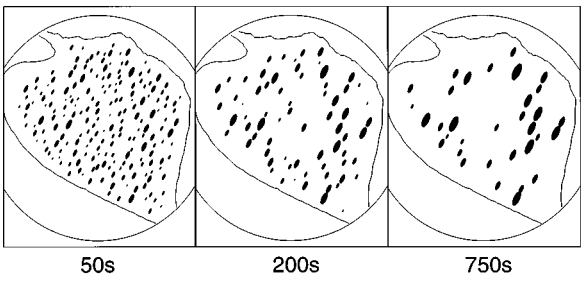

FIG. 9. The first panel shows the abstract version of the experimental configuration marked in Fig. 8. This configuration was propagated forward in time assuming that the chemical potential of the adatom sea surrounding the islands is uniform and determined by the average island size.

Having established the need for a model that features a high degree of nonuniformity in the chemical potential, we turn to the particularly simple case in which the chemical potential at the site of a given island depends only on its nearest-neighbor islands, determined by the Voronoi construction.[30] To determine this chemical potential, we first model the currents between neighboring islands. To do this, we assume that the current between neighboring pairs of islands is proportional to the difference in the chemical potentials between them. The proportionality constant needs to be consistent with the isolated island decay rate of Eq. (4.3) when one of the islands becomes small and be symmetrically determined by the geometry of both islands. To satisfy these constraints in our model the current $J_{i,j}$ from island i to nearest neighbor island j was taken to be

$$J_{i,j}=\frac{\Gamma}{\omega kT}\frac{C_iC_j}{C_i+C_j}\frac{\alpha_{i.j}}{2\pi}(\mu_i-\mu_j), \tag{7.1}$$

where $\alpha_{i,j}$ is the angle subtended by the edge of the Voronoi polygon bisecting the line between islands i and j, yielding $\alpha_{i,j}=\alpha_{j,i}$ and therefore $J_{i,j}=-J_{j,i}$. The current between each pair of islands is geometrically limited by the smaller circumference, which ensures that the current away from a small island reduces to that given by Eq. (4.3) because $\Sigma_j\alpha_{i,j}=2\pi$. From the result for $\mu_{\rm ad}$ found below, the choice in Eq. (7.1) of the geometrical prefactor as $C_iC_j/(C_i+C_j)$ in Eq. (7.1) makes the effective $\mu_{\rm ad}$ of a pair of isolated islands the same, so in some sense this choice attempts to minimize the variations in $\mu_{\rm ad}$, as is required if the adatom diffusion coefficient is large. (In Sec. IX we show that the gradients in $\mu_{\rm ad}$ predicted by this model are indeed reasonable.) However, this exact choice is not critical: replacing $C_iC_j/(C_i+C_j)$ by the smaller of C_i and C_j turns out to have only a slight effect on the simulation discussed below. Weighting the current by the opening angle has the favorable side effect of making the currents insensitive against abrupt changes in the number of neighbors caused by only slight changes in the island positions.

Using the fact that $\Sigma_jJ_{i,j}=dA_i/dt$, and by defining $\mu_{\rm ad}$ for the model by Eq. (4.1), Eq. (7.1) yields a $\mu_{\rm ad}$ surrounding the ith island of

$$\mu_{{\rm ad},i}=\frac{\omega\sqrt{\tilde{\beta}_A\tilde{\beta}_B}}{2\pi}\sum_j\ \alpha_{i,j}\frac{2}{r_i+r_j}, \tag{7.2}$$

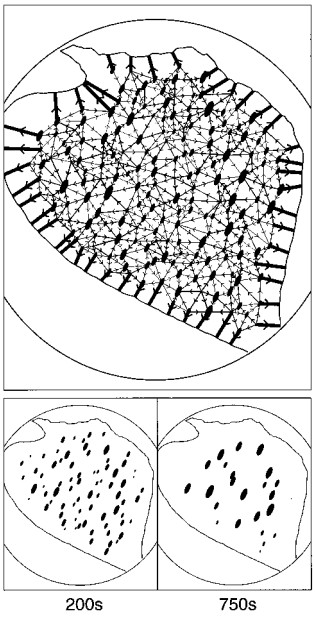

FIG. 10. The upper panel shows the currents between islands determined by comparing the Gibbs-Thomson chemical potential of neighboring islands as described in the text. The width of the lines connecting the islands is proportional to the atomic current between the islands. The subsequent panels show the time development that follows from these currents.

where $r \equiv \sqrt{R_A R_B}$. Thus, in the model, for each neighboring pair of islands, there is a contribution to the chemical potential of the adatom sea that is proportional to the inverse of the mean radius of the pair, similar to the mean-field case. The total effective chemical potential is a weighted average of these that conserves the total island area.

Using Eq. (7.2), the experimental configuration was again propagated forward in time. In this simulation, the bounding step edge was taken to have zero chemical potential: combined with the weighting of the step edge, this choice reproduced the experimentally observed decrease in the total island area. As Fig. 10 shows, we now get very good agreement with experiment. The ratio of dissolution to average growth rate in this model was 5.0, slightly larger than the experimental result. As a result, the value of Γ used in the simulation was chosen to be slightly smaller (3.8/5) to match the experimentally observed rate of increase in average area.

VIII. CHEMICAL POTENTIAL MAPS

The failure of mean-field theory to explain the observed time dependence of ripening implies the existence of significant local variations in the adatom chemical potential. These variations can be directly obtained from the LEEM data: Given our confidence in the validity of Eq. (4.1), we can use it to directly chart out $\mu_{\rm ad}$. Figure 11 shows the maps of $\mu_{\rm ad}$ at 100 and 420 s obtained by measuring $\partial A/\partial t$ for each island and solving Eq. (4.1) for $\mu_{\rm ad}$. The differences between the $\mu_{\rm ad}$ of neighboring islands is usually much less than the differences in the Gibbs-Thomson island chemical potential, i.e., there is a discontinuity in $\mu_{\rm ad}$ at the island edges. This is consistent with the assumption of attachment-limited step-edge kinetics.

Figures 11(c) and 11(d) show the theoretical chemical potentials obtained from the nearest-neighbor model [Eq. (7.2)]. The agreement with Figs. 11(a) and 11(b) is good. As in experiment, the chemical potential is smaller near the bounding step edge. The consistently smaller chemical potential near the bounding step edges causes islands near the boundary to ripen sooner than those in the center. As a result, islands near the center tend to be smaller than average. The chemical potential gradient drives a current in the adatom sea towards the bounding step edge. At 420 s the overall chemical potential is lower than at 100 s and the gradients towards the step edge are smaller, consistent with the approach to equilibrium.

Most of the observed variation of the chemical potential is due to the presence of the bounding step edge: mean-field theory would work better for a larger system, where more islands are further from the boundary. However, the way the system reacts to the bounding step edge shows clearly the effect of nearest-neighbor island correlations.

To quantify the agreement between theory and experiment, Fig. 12 plots the experimental chemical potentials against those predicted by averaging the Gibbs-Thomson chemical potential of neighboring islands. For almost all of the islands, the theoretical chemical potentials are within the uncertainty of experimental results. The linear correlation coefficient[31] of this plot is 0.51. The probability of such a large value of the linear correlation coefficient occurring if the experimental and theoretical chemical potentials were uncorrelated for the 97 analyzed islands is very small: approximately 10^{-6}.[31]

IX. ROLE OF TERRACE DIFFUSION

By measuring the flux of adatoms towards the bounding step edge, the observed chemical potential gradients can be used to estimate the adatom diffusion constant. At 100 s the rate of decrease loss of total island area is approximately 2×10^2 nm^2/s, or 680 dimers/s. The bounding step edge has a length of approximately 1530 nm, giving a flux density j towards the step edge of 0.4 dimers/nm s. This flux is related to the chemical potential gradients towards the step edge through $j = Dc_0\nabla\mu_{\rm ad}/kT$, where c_0 is the equilibrium adatom concentration in the absence of islands and step edges. Estimating the chemical potential gradient towards the step edge from Fig. 11(a) to be 10^{-4} meV/nm at 100 s and assuming that D is approximately isotropic,[32] this gives a value of c_0D of 3×10^5/s. With the definition of the surface mass self-diffusion constant D_M as $c_0D\omega$, this yields a value of D_M of order 7×10^4 nm^2/s. This is in good agreement with the value of $D_M \approx 4.5\times10^4$ nm^2/s extrapolated from studies of the time evolution of periodic step arrays by Keeffe *et al.*[33]

If we assume that atoms are diffusing in units of dimers, then the value of $Dc_0 \approx 3\times10^5$/s is approximately the number of collisions per second of dimers with the step edge. The step mobility at 670 °C of $\Gamma \approx 56$ nm^3/s divided by $\omega^{3/2} = [\sqrt{2}(0.38)\ \text{nm}]^3$ is approximately the number of dimer attachments per second. So for every 900 collisions of a dimer with a step edge, there is approximately one change of the step edge. This large ratio is consistent with the step kinetics being attachment limited on small length scales. For

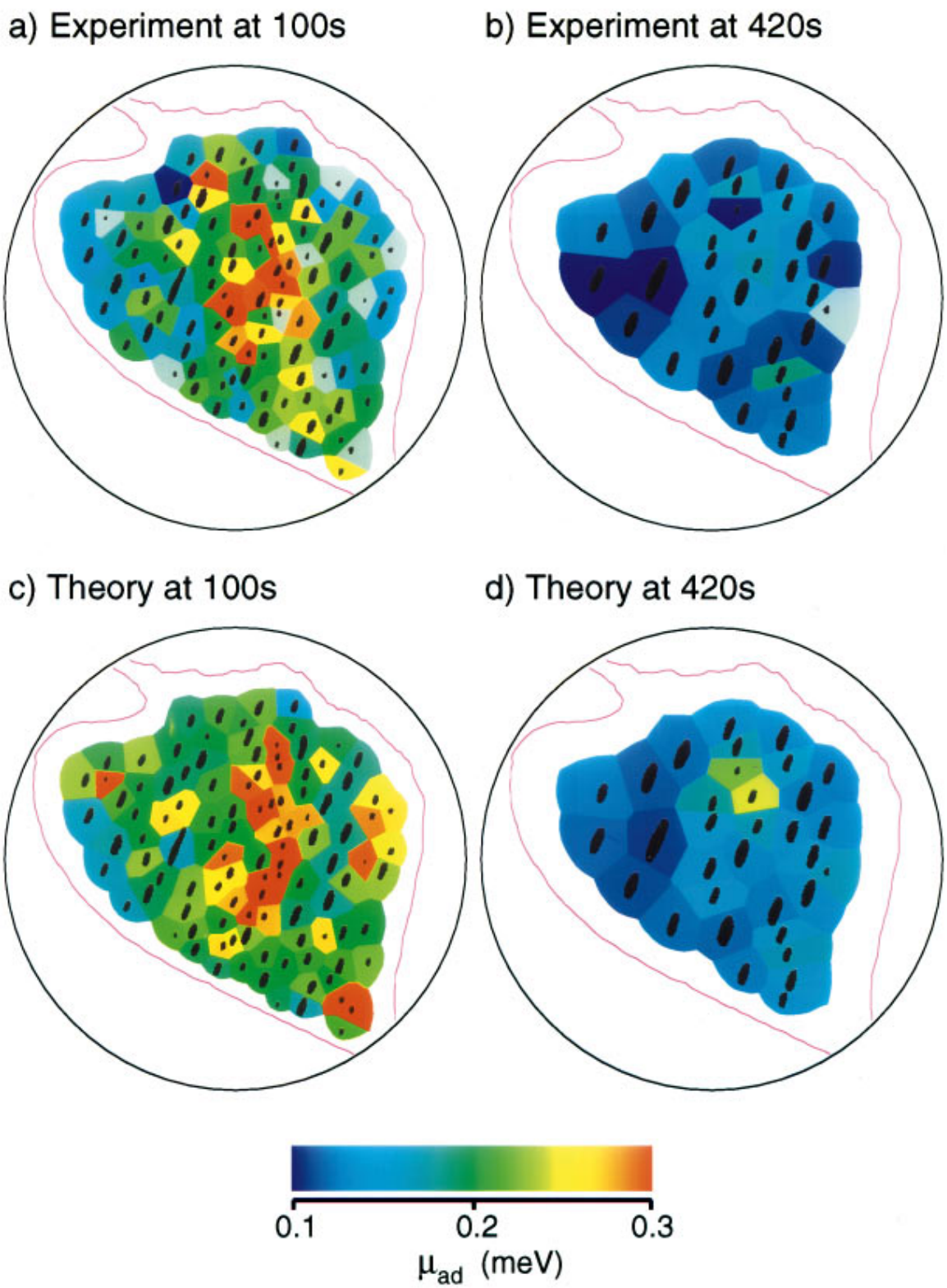

FIG. 11. By measuring the change in area of islands as shown in Fig. 2 with time, the effective chemical potential μ_{ad} of the environment of each island can be determined. These chemical potentials are charted in panels (a) and (b). For small islands sizes, the rate becomes insensitive to the chemical potential. These regions are marked in gray. Panels (c) and (d) show the chemical potential maps calculated using the nearest-neighbor island model of Fig. 10 for the same two times.

sufficiently large islands, dissolution and ripening rates are always expected to be diffusion limited.[11] However, the crossover radius[11] is $R_c = Dc_0\omega^2/\Gamma$, which from the above quoted values is around 500 nm, much larger than the islands studied in the ripening experiment.

Finite diffusion can limit the influence of islands far apart from each other in two ways. For one, there is a finite diffusion length $\sqrt{Dt}$ associated with it. From the above estimate

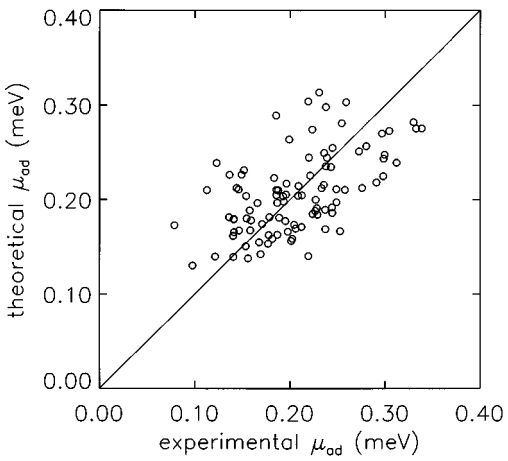

FIG. 12. Theoretical chemical potentials plotted against the experimental measurements at 100 s. If the nearest-neighbor model of Fig. 10 were perfectly correct, the circles would lie on the straight line through the origin.

of Dc_0, if c_0 were $10^{-3}/\omega$, the diffusion length exceeds the size of the terrace in less than one second. Thus it seems unlikely that a finite diffusion length effects the evolution of the island configuration on the time scale of the experiment.[34]

The other way that finite diffusion could localize the interaction between islands is in conjunction with the screening of diffusion fields caused by neighbor islands acting as sources and sinks of adatoms.[6,10] For infinitely fast diffusion this screening would be ineffective. In the following paragraphs we will give an estimate for the effectiveness of screening given the diffusion constant determined above, showing that this mechanism is the physical reason for the nearest-neighbor correlation.

For our discussion, we assume a homogeneous ''screening medium,''[6,10] which averages the effect of an hexagonal array of islands of size $R_{A,B}$ and nearest-neighbor distance d, resulting in a coverage $\phi=(2\pi/\sqrt{3})\langle R_A\rangle\langle R_B\rangle/d^2$. Now imagine a large-scale deviation of the adatom chemical potential from it equilibrium value of $\mu_{\rm ad}=\mu(R_{A,B})$. The islands will become net sources or sinks of adatoms. The change in local concentration caused by the islands emitting or absorbing islands is the number of islands per unit area times the rate of change of the number of atoms of the average island:

$$\frac{\partial c}{\partial t}=-\left(\frac{1}{\omega}\frac{\partial A}{\partial t}\bigg|_{\langle R\rangle}\right)\frac{\phi}{\pi\langle R_A\rangle\langle R_B\rangle}=-\left(\frac{1}{\omega}\frac{\partial A}{\partial t}\bigg|_{\langle R\rangle}\right)\frac{2}{\sqrt{3}}\frac{1}{d^2}. \tag{9.1}$$

To compute $\partial A/\partial t$ we use Eq. (4.1) and assume that the adatom gas is ideal and dilute so that the chemical potential is $\mu_{\rm ad}(\mathbf{r})=kT\ \ln[c(\mathbf{r})/c_0]\approx kT[c_0-c(\mathbf{r})]/c_0$, where $c(\mathbf{r})$ is the spatial dependence of the perturbed adatom concentration. Then Eq. (9.1) becomes

$$\frac{\partial c}{\partial t}=-\sqrt{\frac{3}{2}}\frac{1}{d^2}\frac{1}{c_0\omega^2}\sqrt{\frac{\langle R_A\rangle^2+\langle R_B\rangle^2}{2}}[c(\mathbf{r})-\langle c\rangle], \tag{9.2}$$

where $\langle c\rangle$ is the average adatom concentration determined by the average island radius. In steady state this rate of change in concentration must be balanced by terrace diffusion, leading to a Helmholtz equation for the adatom concentration:

$$D\nabla^2[c(\mathbf{r})-\langle c\rangle]-\frac{D}{\xi^2}[c(\mathbf{r})-\langle c\rangle]=0. \tag{9.3}$$

The screening length ξ is given by

$$\frac{\xi^2}{d^2}=\sqrt{\frac{3}{4\pi}}\left[\frac{1}{2}\left(\frac{\langle R_A\rangle}{\langle R_B\rangle}+\frac{\langle R_B\rangle}{\langle R_A\rangle}\right)\right]^{-1/2}\frac{R_c}{\sqrt{\langle R_A\rangle\langle R_B\rangle}}$$
$$\approx\frac{1}{9}\frac{R_c}{\sqrt{\langle R_A\rangle\langle R_B\rangle}}, \tag{9.4}$$

where R_c is the crossover radius introduced above at which ripening changes its character from attachment-detachment limited to diffusion limited. If ξ is equal to *or less than* d, then the nearest neighbors will effectively shield the diffusion field of each island. Using the values of D deduced above, we find that R_c is approximately $10\sqrt{\langle R_AR_B\rangle}$. So the estimated values of D is small enough to account for the nearest-neighbor screening, yet large enough that ripening occurs well into the attachment-detachment limited regime.

While we have discussed possible reasons for the success of the nearest-neighbor model above, we will now introduce a numerical simulation based on approximately solving the diffusion equation with attachment-detachment limited step-edge kinetics. This simulation also reproduces the experimental results, demonstrating that these ingredients can fully describe the ripening and lead to an effective nearest-neighbor interaction for the given balance between attachment limited step-edge kinetics and diffusion. We assume circular islands and isotropic diffusion ($\mathbf{j}=-D\nabla c$). The unknowns are the island growth rates $q_i=dA_i/dt$. Assuming that the corresponding adatom fluxes originate from point sources, the steady-state adatom concentration is given by

$$c(\mathbf{r})=c_B(\mathbf{r})-\frac{1}{2\pi\omega D}\sum_i q_i\ln(|\mathbf{r}-\mathbf{r}_i|/a), \tag{9.5}$$

with $\nabla^2c_B(\mathbf{r})=0$ on the terrace. The attachment-detachment rate equation must be satisfied for every island. Using $\mu_{\rm ad}=kT\ln[c(\mathbf{r})/c_0]\approx kT[c(\mathbf{r})-c_0]/c_0$ yields a linear equation in q_i for every island. (The concentration at the edge of island i was determined by evaluating its own logarithmic term at $|\mathbf{r}-\mathbf{r}_i|=R_i$, the island's radius, and all other terms at $\mathbf{r}=\mathbf{r}_i$.)

If $c_B(\mathbf{r})$ could be expressed as a linear function of q_i the problem would reduce to a large linear system that could be solved in a straightforward way. Here, for simplicity, we invoke the boundary condition at the bounding step. First of all, the edge chemical potential can be taken to be zero everywhere on the bounding edge. Second, the contribution to the adatom concentration due to the islands, the attachment current and therefore $c_B(\mathbf{r})$ can be assumed to be similar at all places on the bounding edge in a first approximation. This

approximation, taking $c_B(\mathbf{r})$ to be constant on the bounding edge, makes it constant everywhere on the terrace because $\nabla^2 c_B(\mathbf{r})=0$.

At the bounding edge, the attachment current must be equal to the detachment current. Picking one location on the edge (as stated above, all locations have similar currents and chemical potentials) we get a boundary condition yielding c_B as a linear expression in q_i. Solving the linear system gives the island growth rates, dependent on the given configuration, temperature, step-edge stiffnesses $\beta_{A,B}$, mobility Γ, and diffusion constant $\omega D c_0$. The experimental evolution of the configuration is reproduced best with $\omega D c_0 = 3\times 10^4$ nm^2/s, which is in good agreement with the values discussed above. The derived chemical potential map is virtually identical to the chemical potential map from the nearest-neighbor model.

X. CONCLUSION

We have been able to account for, in detail, the time evolution of a large number of islands by considering step-edge attachment kinetics and diffusion in the adatom sea. The time dependence of an individual island is attachment-detachment limited, driven by the difference between the chemical potential of the island and the surrounding adatom sea. The length scale over which the adatom sea equilibrates with the islands is, however, limited by diffusion, giving rise to strong nearest-neighbor correlations during the ripening. The values obtained for the isolated island dissolution rate and for the surface diffusion coefficient are in good agreement with previous studies of step capillary wave motion and the decay of surface gratings by surface diffusion, capturing this variety of phenomena in a single, coherent framework.

ACKNOWLEDGMENTS

WT acknowledges a grant from the Max-Planck Gesellschaft. N.B. was supported by the NSF under Grant No. DMR91-03031. We thank Mark Reuter for his assistance with the experiments and Pita Atala for useful and insightful comments on the manuscript.

APPENDIX

Here we give the mean-field expressions for the time dependence of the island size distribution for the detachment-limited Ostwald ripening of 2D islands. The analogous expressions for diffusion-limited kinetics appear in Ref. 9. The detailed derivation of the distribution is a slight modification of arguments presented in Refs. 16 and 35 for 3D islands; the result is the same as for the 2D grain evolution model of Ref. 36.

Start by slightly rewriting Eq. (4.1), by introducing the critical island size $r_c(t)$:

$$\dot{r}\equiv\frac{dr}{dt}=-\frac{B}{r}\left(1-\frac{r}{r_c}\right), \tag{A1}$$

where $B\equiv(\Gamma/kT)\sqrt{\tilde{\beta}_A\tilde{\beta}_B(R_A/R_B+R_B/R_A)/2}$ and $r\equiv\sqrt{R_A R_B}$. Now consider the probability distribution $f(r,t)$ of islands of size r at time t. There is a continuity equation for this distribution: the rate of change of the number of islands of a particular size must be balanced by how quickly the radius of these islands are changing. Thus

$$\frac{\partial f(r,t)}{\partial t}+\frac{\partial}{\partial r}[\dot{r}f(r,t)]=0. \tag{A2}$$

We suppose that the sum of all of the island areas is conserved (only an approximation in the present case, because of the loss of atoms to the step edge). At long times, the solution to Eq. (A2), given Eq. (A1), and the constraint of fixed island area is[36]

$$f(r,t)=\begin{cases}\dfrac{\rho}{2}\left(\dfrac{2}{2-\rho}\right)^4\exp\left(\dfrac{-2\rho}{2-\rho}\right) & \text{if } \rho<2\\ 0 & \text{if } \rho>2,\end{cases} \tag{A3}$$

where $\rho(t)=r/r_c(t)$. This distribution is compared with experiment in Fig. 4. Integrating over this distribution shows that the average radius is equal to r_c. This property was used in computing the value of r_c used in the simulations shown in Fig. 10. [Another way of establishing the equality between r_c and $\langle r\rangle$ is to note that the sum of the rates of change of each island area A_i is zero. Then, from Eq. (A1), $\Sigma_i \partial A_i/\partial t = 0 = 2\pi B\Sigma_i(1-r_i/r_c)\propto 1-\langle r\rangle/r_c$.]

The value of $r_c(t)$ in Eq. (A3) is[36]

$$r_c^2(t)=\langle r(t)\rangle^2=\langle r(0)\rangle^2+Bt/2. \tag{A4}$$

This is consistent with the linear time dependence of the average island area shown in Fig. 3. Because integrating Eq. (A3) gives $\langle r^2\rangle = 1.109\,37\langle r\rangle^2$,

$$\langle A(t)\rangle=\frac{1.109\,37B\pi}{2}t+\langle A(0)\rangle. \tag{A5}$$

Thus, within mean-field theory, the rate of increase of the average area with time is $\sim 1/3.6$ of the rate of decrease of an individual small island. As discussed in the text, this is close to the experimentally observed ratio.

*Present address: Sandia National Laboratories, Livermore, CA 94551.

†Present address: Institut für Experimentalphysik, Freie Universtität Berlin, Arnimallee 14, D-14195 Berlin, Germany.

[1] P.W. Voorhees, Annu. Rev. Mater. Sci. **22**, 197 (1992); J. Stat. Phys. **38**, 231 (1985).

[2] M.G. Lagally, R. Kariotis, B.S. Swartzentruber, and Y.W. Mo, Ultramicroscopy **31**, 87 (1989); M.G. Lagally, Y.-W. Mo, R. Kariotis, B.S. Swartzentruber, and M.B. Webb, in *Kinetics of Ordering and Growth at Surfaces*, edited by M.G. Lagally (Plenum, New York, 1990), p. 145.

[3] N.C. Bartelt, R.M. Tromp, and E.D. Williams, Phys. Rev. Lett. **73**, 1656 (1994); N.C. Bartelt and R.M. Tromp, preceding paper, Phys. Rev. B **54**, 11 731 (1996).

[4] W. Theis, N.C. Bartelt, and R.M. Tromp, Phys. Rev. Lett. **75**, 3328 (1995).

[5] I.M. Lifshitz and V.V. Slyozov, J. Chem. Solids **19**, 35 (1961).

[6] A.D. Brailsford and P. Wynblatt, Acta Metall. **27**, 489 (1979).

[7] H. Fischmeister and G. Grimvall, in *Sintering and Related Phenomena*, edited by G.C. Kuczynski (Plenum, New York, 1973), p. 119.

[8] M. Marder, Phys. Rev. A **36**, 858 (1987).

[9] T.M. Rogers and R.C. Desai, Phys. Rev. B **39**, 11 956 (1989).

[10] J.A. Marqusee, J. Chem. Phys. **81**, 976 (1984).

[11] M. Zinke-Allmang, L.C. Feldman, and M.H. Grabow, Surf. Sci. Rep. **16**, 377 (1992).

[12] O. Krichevsky and J. Stavans, Phys. Rev. Lett. **70**, 1473 (1993).

[13] W. Telieps and E. Bauer, Ultramicroscopy **17**, 57 (1985); R.M. Tromp and M.C. Reuter, in *Interface Dynamics and Growth*, edited by K.S. Liange, M.P. Anderson, R.F. Bruinsma, and G. Scoles, MRS Symposia Proceedings No. 237 (Materials Research Society, Pittsburgh, 1992), p. 349.

[14] W.K. Pratt, *Digital Image Processing* (Wiley, New York, 1991).

[15] Similar variations in individual particle ripening rates have also been directly observed by P.W. Voorhees and R.J. Schaefer, Acta Metall. **35**, 327 (1987).

[16] C. Wagner, Z. Electrochem. **65**, 581 (1961).

[17] A.A. Chernov, Usp. Fiz. Nauk **73**, 277 (1961) [Sov. Phys. Usp. **4**, 116 (1961)].

[18] We are describing the island dissolution by a single step mobility Γ, despite the fact that the step structure changes around the circumference of the island. This is justified because the islands retain their equilibrium shape as they are dissolving, perhaps because of diffusion along the edges of the islands. Because of the orientational dependence of step structure, this mobility will be an average over the orientational dependence of the mobility and step free energies of isolated straight steps. This, in principle, makes a direct comparison of the mobility extracted from island evolutions to the mobility of individual straight steps ambiguous. Fortunately, however, at these high temperatures the step mobility is observed to be approximately isotropic (Ref. 3).

[19] N.C. Bartelt, J.L. Goldberg, T.L. Einstein, and E.D. Williams, Surf. Sci. **273**, 252 (1992).

[20] N.C. Bartelt, J.L. Goldberg, T.L. Einstein, E.D. Williams, J.C. Heyraud, and J.J. Métois, Phys. Rev. B **48**, 15 453 (1993).

[21] N.C. Bartelt, T.L. Einstein, and E.D. Williams, Surf. Sci. **312**, 411 (1994).

[22] In making this estimate we assume that the individual dimers are randomly attaching and detaching from the step edge. At low temperature, STM observations suggest that dimers attach and detach from the step edge in pairs (Refs. 25, 27, and 28). If this behavior persisted to high temperature, then only the random attachment rate of pairs of dimers would be random. To explain the observed values of Γ, the dimer attachment rates would have to be a factor of $2\sqrt{2}$ lower than given in the text because the mobility is proportional to the cube of the size of the entity, which is randomly attaching and detaching. This difference has no qualitative affect on our conclusions. If the coordinated participation of pairs of dimers were required to change the step edge position, it might account for attachment-limited step edge kinetics. For the case of Ag islands on Ag(111), where there is no such complexity associated with step edge attachment and detachment, diffusion-limited dissolution of islands has recently been observed [K. Morgenstern, G. Rosenfeld, and G. Comsa, Phys. Rev. Lett. **76**, 2113 (1996)].

[23] If the detachment rate were comparable to the random exchange rate, then it might be difficult for the step structure to be in local equilibrium and the island step edge would exhibit kinetic roughening.

[24] Depending on how fast diffusion is across step edges, the existence of different attachment or detachment rates from terraces above and below the step edges could also effect the comparison between the step capillary wave and island dissolution mobilities.

[25] H.J.W. Zandvliet, H.B. Elswijk, and E.J. van Loenen, Surf. Sci. **272**, 264 (1992).

[26] C. Pearson, B. Borovsky, M. Krueger, R. Curtis, and E. Ganz, Phys. Rev. Lett. **74**, 2710 (1995).

[27] N. Kitamura, B.S. Swartzentruber, M.G. Lagally, and M. B. Webb, Phys. Rev. B **48**, 5704 (1993).

[28] B.S. Swartzentruber and M. Schact, Surf. Sci. **322**, 83 (1995).

[29] These simulations are completely deterministic. We neglect, for example, the stochastic effects caused by random step edge fluctuations. See F.-P. Ludwig, J. Schmelzer, and J. Bartels, J. Mater. Sci. **29**, 4852 (1994) for a discussion of the effects of thermal noise on the ripening.

[30] To compute the Voronoi polygons we used the algorithm of I.K. Crain, Comput. & Geosci. **4**, 131 (1978).

[31] P.R. Bevington, *Data Reduction and Error Analysis for the Physical Sciences* (McGraw-Hill, New York, 1969).

[32] At low temperature, STM experiments show that diffusion of atoms, ad-dimers, and vacancies on the terraces are highly anisotropic. Whether this anisotropy persists to the high temperatures of this experiment is not known. Direct evidence that the anisotropy is not large, or at least not important, is the approximately isotropic denuded zone close to the bounding step edges (although this is also related to the observed isotropy of the step mobilities).

[33] M.E. Keeffe, C.C. Umbach, and J.M. Blakely, J. Phys. Chem. Solids **55**, 965 (1994).

[34] The large diffusion length does not imply that the adatom chemical potential should be in equilibrium with the bounding step edge. This issue is addressed theoretically by C.W.J. Beenakker and J. Ross, J. Chem. Phys. **83**, 4710 (1985), and experimentally by G.R. Carlow and M. Zinke-Allmang, Can. J. Phys. **72**, 812 (1994).

[35] B.K. Chakraverty, J. Phys. Chem. Solids **28**, 2401 (1967).

[36] M. Hillert, Acta Metall. **13**, 227 (1965).